

Direct simulation of a zero-pressure-gradient turbulent boundary layer up to  $Re = 6650$

This article has been downloaded from IOPscience. Please scroll down to see the full text article.

2011 J. Phys.: Conf. Ser. 318 022023

(<http://iopscience.iop.org/1742-6596/318/2/022023>)

View [the table of contents for this issue](#), or go to the [journal homepage](#) for more

Download details:

IP Address: 138.4.116.84

The article was downloaded on 13/01/2012 at 11:22

Please note that [terms and conditions apply](#).

# Direct simulation of a zero-pressure-gradient turbulent boundary layer up to $Re_\theta = 6650$

Juan Sillero<sup>1</sup>, Javier Jiménez<sup>1</sup>, Robert D. Moser<sup>2</sup> and Nicholas P. Malaya<sup>2</sup>

<sup>1</sup> School of Aeronautics, Universidad Politécnica de Madrid, 28040 Madrid, Spain

<sup>2</sup> Dept. Mech. Eng. and Inst. for Computat. Eng. and Sciences, U. of Texas, Austin, TX 78735, USA

E-mail: sillero@torroja.dmt.upm.es

**Abstract.** A direct simulation of an incompressible zero-pressure-gradient turbulent boundary layer over a flat plate is performed in  $Re_\theta = 1100 - 6650$  ( $Re_\tau \approx 2025$ ), matching the range of the available numerical channels. The logarithmic region and the separation of scales are clearly observed. Proper turbulent inflow conditions, key in boundary layers, are generated by an auxiliary simulation at lower resolution and Reynolds number. Results are in agreement with existing numerical and experimental data sets.

## 1. Introduction

Turbulent boundary layers are subjects of intensive research because of their technological importance. High-quality direct simulations have recently become possible for wall-bounded flows, mainly channels, featuring an appreciable logarithmic layer. Their role is essential to understand the kinematics and dynamics of the turbulent structures. Turbulent boundary layer Reynolds numbers have increased more slowly than in channels, because the streamwise inhomogeneity is harder to compute, and because of the difficulty of prescribing correct inflow conditions. Simulations have appeared in the past few years at Reynolds numbers up to  $Re_\theta = 2100$  in [Simens, Jiménez, Hoyas & Mizuno, 2009; Jiménez, Hoyas, Simens & Mizuno, 2010], and  $Re_\theta = 4060$  in [Schlatter & Örlü, 2010]. They show differences with respect to channels, which are also seen in experiments, but lack a good representation of the logarithmic layer. Therefore, the purpose of the present simulation is to extend the Reynolds number range to  $Re_\theta \approx 6500$  ( $Re_\tau = 2000$ ), comparable to the largest available simulations of numerical channels.

## 2. Methods

The boundary layer is simulated in a parallelepiped over a flat plate with periodic boundary conditions spanwise and non-periodic in streamwise direction. The turbulent inflow is generated using the method in [Lund, Wu & Squires, 1998], in which the velocities from a reference downstream plane are used to create the incoming turbulence. The effect is equivalent to the trip used in experiments [Simens, Jiménez, Hoyas & Mizuno, 2009], in that the flow must recover from an unrealistic condition to converge to an asymptotic state. The proper scale to measure the length required for that recovery is the distance,  $L_{to} = U_\infty^+ \delta$ , by which eddies are advected during

a turnover time  $\delta/u_\tau$ , where  $\delta$  is the boundary-layer thickness,  $u_\tau$  is the local friction velocity and  $U_\infty$  is the free-stream velocity. The effective dimensionless length of the computational box can then be defined as  $\tilde{x} = \int_0^x dx/(\delta U_\infty^+)$ . It was found in [Simens, Jiménez, Hoyas & Mizuno, 2009] that the accommodation length for most flow scales is at least  $\tilde{x} = 1$ . That remains true for the all but the largest fluctuations, but experiments during the present simulation convinced us that some properties of the mean profile, especially the shape factor, do not converge until  $\tilde{x} \approx 4$ . Unfortunately, the ratio  $\delta_{to}/\delta$  increases with the Reynolds number, because  $u_\tau$  decreases, and simulations become increasingly expensive. For example, table 1 includes two of the cases run for this simulations. The first one,  $BL^I$ , spans  $Re_\theta = 2580 - 6340$  in a box approximately twice longer ( $50\delta$ ) than those used in channels, but its mean profile has not reached equilibrium by the end of the box,  $\tilde{L}_x \approx 2.57$ .

**Table 1.** Parameters of the turbulent boundary layers cases considered.  $L_x, L_y$  and  $L_z$  are the box dimensions. The momentum thickness  $\theta$  is taken at the middle of the box.  $\tilde{L}_x$  is the effective dimensionless computational box length.  $N_x, N_y$  and  $N_z$  are the grid sizes.

Case	$Re_\theta$	$(L_x, L_y, L_z)/\theta$	$\tilde{L}_x$	$\Delta x^+, \Delta y^+, \Delta z^+$	$N_x, N_y, N_z$
$BL^I$	2580-6340	$534 \times 30 \times 67$	2.57	$6.10 \times 0.30 \times 4.15$	$16385 \times 711 \times 4096$
$BL_1^{II}$	1100-2970	$481 \times 47 \times 191$	2.61	$13.00 \times 0.32 \times 7.28$	$3585 \times 315 \times 2560$
$BL_2^{II}$	2780-6650	$547 \times 29 \times 84$	2.68	$7.00 \times 0.32 \times 4.07$	$15361 \times 535 \times 4096$

Since only the largest scales appeared to be involved, the problem was solved using an auxiliary lower-resolution simulation,  $BL_1^{II}$ , run in synchrony with the high-resolution main layer. That auxiliary boundary layer uses the rescaling technique to generate its inflow, and is used to feed the inflow of the main simulation,  $BL_2^{II}$ , from a plane near the end of  $BL_1^{II}$  at  $\tilde{x} \approx 2.39$ . The lower resolution of  $BL_1^{II}$  is justified because its main purpose is to allow the large scales to reach equilibrium. Only a moderate under-resolution is required. Even a linear factor of 2 reduces the computational cost of the auxiliary simulation to about 10% of the main one. In fact, the fluctuation profiles of the auxiliary simulation appear essentially correct, and the intermediate spectrum of figure 3(a) belongs to that case. Note that, since  $BL_2^{II}$  does not use a rescaling technique, its accommodation length is very short, and most of its domain can be considered valid.

### 3. Results

The preliminary statistics presented here are collected over a period of  $Tu_\tau/\delta = 3$  eddy turnovers, measured at the middle of the domain of  $BL_2^{II}$ . This simulation is still in production stage, and 17 eddy turnovers are expected to be collected.

Figure 1(a)-(b) shows the friction coefficient  $c_f = 2/U_\infty^{+2}$  and the shape factor  $H = \delta^*/\theta$  as a function of  $Re_\theta$  compared with available experimental [De Graaff & Eaton, 2000; Osterlund, Johansson, Nagib & Hites, 2000; Purtell, Klebanoff & Buckley, 1981; Erm & Joubert, 1991] and numerical data sets [Schlatter & Örlü, 2010; Simens, Jiménez, Hoyas & Mizuno, 2009]. The present simulation covers a fairly large extent of Reynolds numbers,  $Re_\theta = 1100 - 6650$ , approximately equivalent to channels in the range  $Re_\tau = 440 - 2025$  as shown in figure 2(e). Tripping techniques are commonly used to trigger turbulence, either in experiments or numerical simulations, and as a consequence, accommodation lengths of  $O(\tilde{x})$  are needed. This can be seen in the integral parameters  $c_f$  and  $H$ . Experiments in [Erm & Joubert, 1991] were tripped at

low Reynolds number by wire, grid and pins, resulting in high scatter up to about  $Re_\theta \approx 1500$ . Numerical simulations in [Simens, Jiménez, Hoyas & Mizuno, 2009], as well as the present one, show the effect of tripping by means of the rescaling technique, resulting in a high  $c_f$  and low  $H$ . These deviated values last up to distances of  $\tilde{x}$  between three and four, to finally settle in agreement with the rest of experimental and numerical data sets. This effect is especially severe at high Reynolds numbers, in which the accommodation length can be as long as the entire numerical domain or the experimental analysis region.

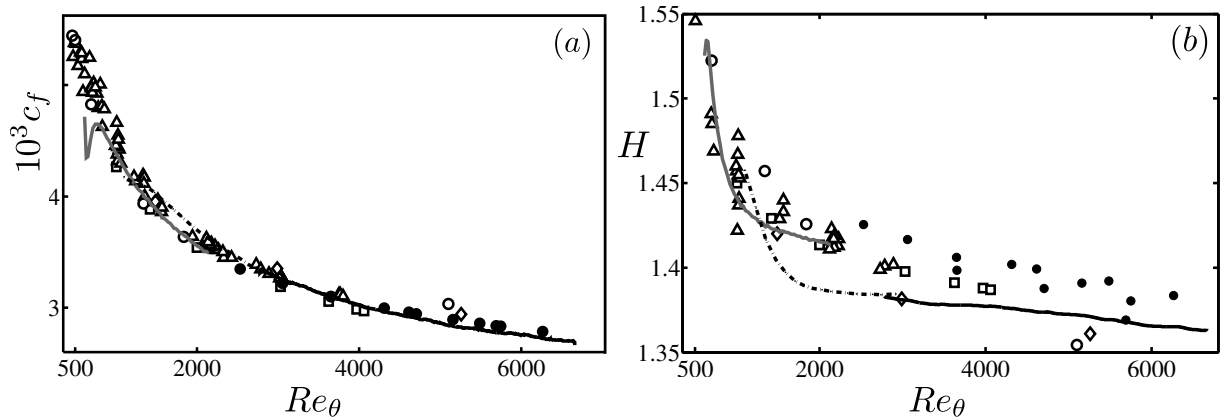


**Figure 1.** Friction coefficient (a) and shape factor (b) versus  $Re_\theta$  number. Symbols are experiments by [De Graaff & Eaton, 2000],  $\diamond$ ; by [Purtell, Klebanoff & Buckley, 1981],  $\circ$ ; [Erm & Joubert, 1991],  $\triangle$ ; and [Osterlund, Johansson, Nagib & Hites, 2000],  $\bullet$ ; and numerical simulations by [Schlatter & Örlü, 2010],  $\square$ . Lines are for the present simulation  $BL_1^{II}$ , --- and  $BL_2^{II}$ , —; and for [Simens, Jiménez, Hoyas & Mizuno, 2009], —

In the present simulation, the purpose of the auxiliary  $BL_1^{II}$  is to provide realistic inlet conditions for  $BL_2^{II}$ , as already discussed. By the end of  $BL_1^{II}$ , i.e. at the beginning of  $BL_2^{II}$ , the large structures have covered about  $\tilde{x} \approx 2.6$  and the values of  $c_f$  are settling into agreement with experimental data. Shape factor also falls within the scatter of the experiments.

Figure 2(a)-(d) presents mean and fluctuation velocity profiles from the present simulation compared with some of the experimental and numerical data sets used for figure 1, in the range of  $Re_\theta = 4060 - 5160$  ( $Re_\tau \approx 1320 - 1616$ ), and it shows excellent agreement. Small scales converge to nominal values within an eddy turn-over, approximately in a distance of  $22\delta_{99}^{inlet}$  from the inlet.  $BL_1^{II}$  velocity fluctuations are essentially correct through the entire domain, with the exception of the inlet accommodation length seen in figure 2(e). Also presented in figure 2 are the data from the numerical channel simulation  $Re_\tau = 2000$  [Hoyas & Jiménez, 2006] for the velocity fluctuations. While the maximum of  $u'^+$  agrees with the boundary layer fluctuations, the transverse velocity fluctuations,  $v'^+$  and  $w'^+$ , do not, and are higher for the boundary layers. This was already noted by [Hoyas & Jiménez, 2008], although using boundary layer simulations at relatively low  $Re_\tau$ . Figure 2(e) presents the maximum velocity fluctuations over the range  $Re_\tau = 500 - 2000$  compared with channels at  $Re_\tau = 180, 550, 950$  and  $2000$ . Both boundary layers and channels exhibit a small Reynolds number dependence in their maximum intensities, failing the classical scaling with  $u_\tau$  near the wall, as already discovered by [De Graaff & Eaton, 2000] in a comparative study of boundary layers. In the buffer layer the squared intensities should be proportional to  $u_\tau^2 \log(Re_\tau)$  when the fluctuations are scaled at fixed  $y^+$  instead of  $y/\delta$ . A slightly different scaling for the velocity fluctuations was investigated by [Jiménez, del Álamo & Flores, 2004] based on spectral arguments, noting that the intensities should be controlled by the

scale ratio between the large structures in the outer region and the smallest ones at the buffer region.

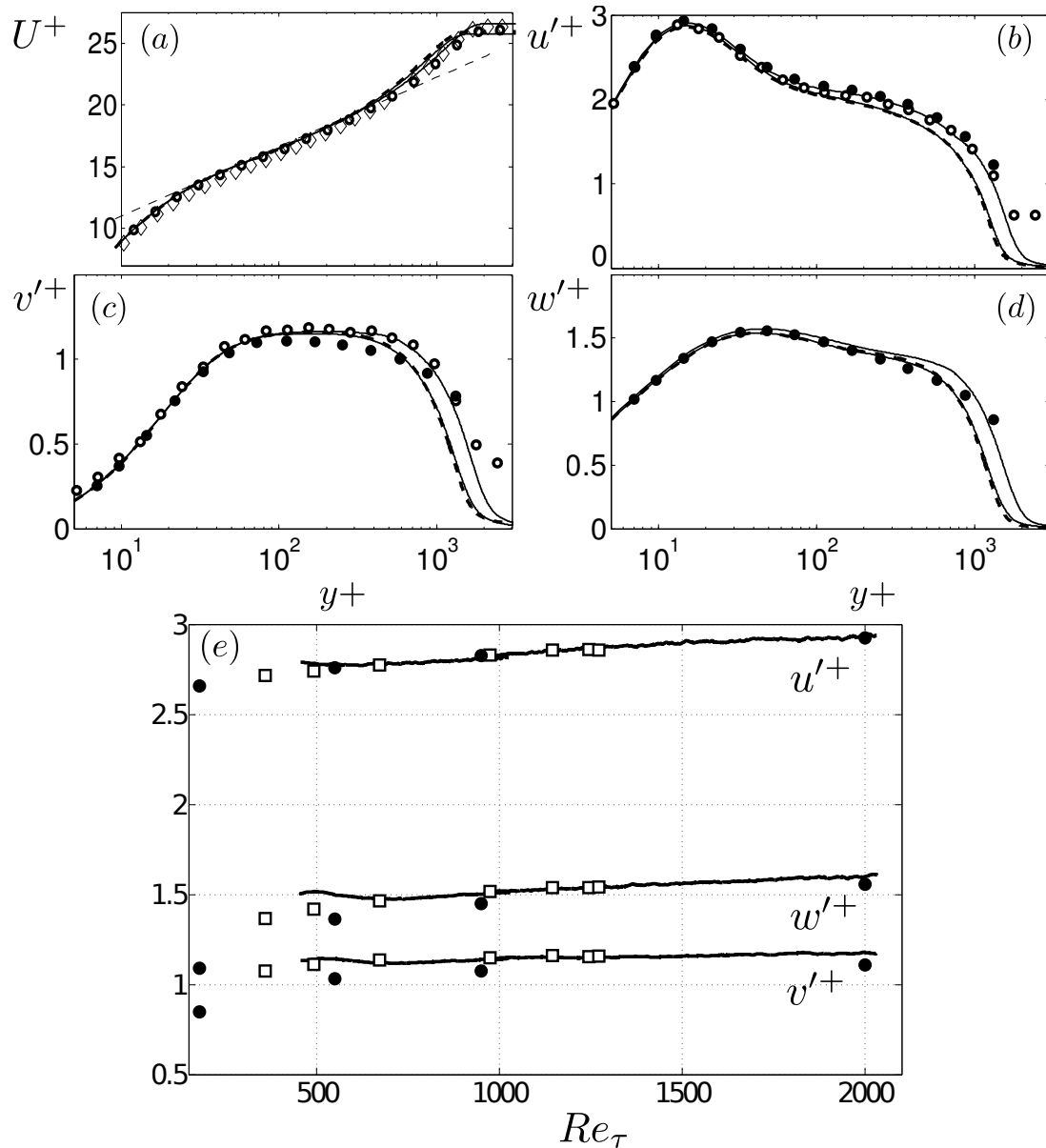


**Figure 2.** (a) Mean streamwise velocity; (b,c,d) root-mean-squared velocity fluctuations. Symbols are: numerical channel [Jiménez, Hoyas, Simens & Mizuno, 2010] at  $Re_\tau = 2003$ ,  $\bullet$ ; boundary layer experiments by [De Graaff & Eaton, 2000] at  $Re_\theta = 5160$ ,  $\circ$ ; and [Osterlund, Johansson, Nagib & Hites, 2000] at  $Re_\theta = 5156$ ,  $\diamond$ . The simulations by [Schlatter & Örlü, 2010] at  $Re_\theta = 4060$  are  $--$ . The law  $\log(y^+)/0.40 + 5$  is  $--$ ; and  $—$  are the present simulation at  $Re_\theta = 4060, 5160$ . (e) Maximum value of the velocity fluctuations versus  $Re_\tau$ .  $\square$  stands for [Schlatter & Örlü, 2010]

Even more interesting are the spectra in figure 3, which shows premultiplied spectral energy  $\Phi_{**} = k_x k_z E_{**}(k_x k_z)$ , where  $k_x$  and  $k_z$  are the wavenumbers in the two wall-parallel directions, with associated wavelengths  $\lambda = 2\pi/k$ , and  $*$  stands for the flow field variables.

A two-dimensional spectra for boundary layer does not exist mathematically, since the only homogeneous direction is spanwise. Spectra is therefore computed as the Fourier transform of the two-points correlation function of each Fourier mode, after symmetrizing it with respect to  $x$ . The largest streamwise wavelength is chosen to be  $\lambda_x \approx 20\delta_{99}$  for all the spectra, in which the boundary layer can be approximately considered as a parallel flow (for  $\Delta_x \approx 20\delta_{99}$ ,  $\Delta\delta/\delta \approx 0.25$ ).

Figure 3(a) compares kinetic spectral density energy  $\Phi_{uu}^+$  for channels at  $Re_\tau = 550 - 2000$  and boundary layers at similar values of  $Re_\tau$  at the buffer layer,  $y^+ = 15$  and for energy levels of 15% and 57% of the total energy. They clearly show the development of the scale separation with the Reynolds number, and also that the layers are slightly shorter than the channels at similar  $Re_\tau$  [Jiménez, Hoyas, Simens & Mizuno, 2010]. On the other hand, they show that the aspect ratio of the large structures in both flows are essentially the same,  $\lambda_x = 10\lambda_z$ .

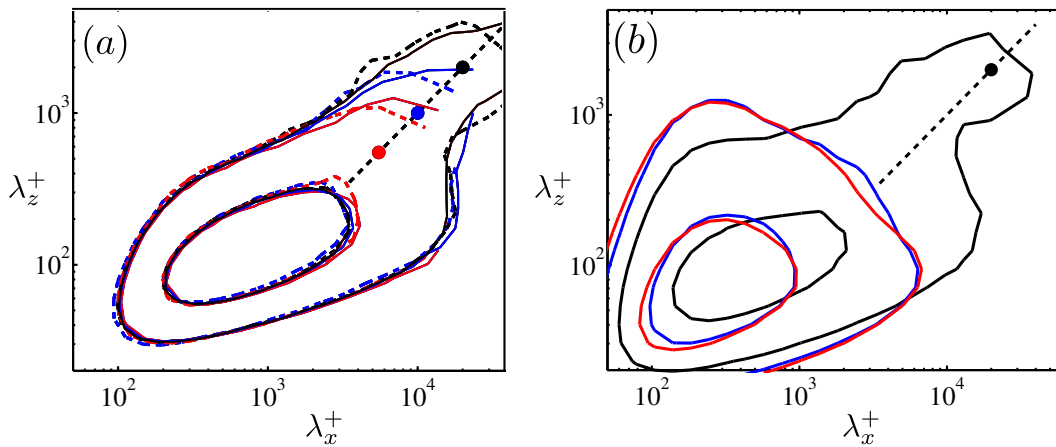


**Figure 3.** (a) Solid lines are two-dimensional spectral densities  $\Phi_{uu}^+$  from channels at  $Re_\tau = 550-2000$  [Hoyas & Jiménez, 2006], and dashed ones those of boundary layers at  $Re_\tau = 550$  [Jiménez, Hoyas, Simens & Mizuno, 2010], and 1000 and 2000 from the present case at the buffer layer,  $y^+ = 15$ , in red, blue, and black respectively. (b) Large scales boundary layer footprint in the vorticity spectral densities  $\Phi_{\omega\omega}^+$  at the viscous sublayer  $y^+ = 5$  (black) and for the buffer layer at  $y^+ = 10 - 15$  (red, blue) at  $Re_\tau \approx 2000$ . In both cases, the straight dashed line is  $\lambda_x = 10\lambda_z$  and dots are  $\lambda_z = Re_\tau$ .

It is interesting to note the effect of the Reynolds number near the wall, due to the large scale inactive motions in the sense of [Townsend, 1976]. This is clearly seen in figure 3(b), in which the spectral enstrophy density  $\Phi_{\omega\omega}^+$  is presented for the boundary layer at  $Re_\tau \approx 2000$  at different wall-normal locations and for enstrophy levels of 8% and 50% of the total. Near the wall, the large scales of the flow are irrotational, because the  $v$  impermeability condition inhibits the Reynolds stresses  $\langle u'v' \rangle$ . This can be seen at the buffer layer locations,  $y^+ = 10$  (red) and  $y^+ = 15$  (blue), where the large scales are missing. The nearest wall value is  $y^+ = 5$  (black), within the viscous layer, and in which the potential flow cannot satisfy the no-slip boundary condition, developing a thin rotational sublayer in which structures are long and wide so the no-slip condition is attained [Hoyas & Jiménez, 2008]. Very near to the wall the vorticity is the velocity gradient in the wall-normal direction, therefore, the vorticity and the velocity spectrum should be proportional at a constant  $y^+$ , as observed in figure 3.

Further analysis of the one-dimensional spectra  $k|E_{**}^{1D}|$  versus  $y$  shows that the streamwise velocities fluctuations structures are long, those for spanwise wide, and those for wall-normal tall. The pressure fluctuations structures are as tall as the wall-normal velocity, but wider and slightly shorter than the streamwise fluctuations ones. This pattern can be observed in figure

4, in which velocity fluctuations of an instantaneous realization of the flow field in the range  $Re_\theta = 5800 - 6600$  ( $Re_\tau \approx 1797 - 2016$ ) are presented.

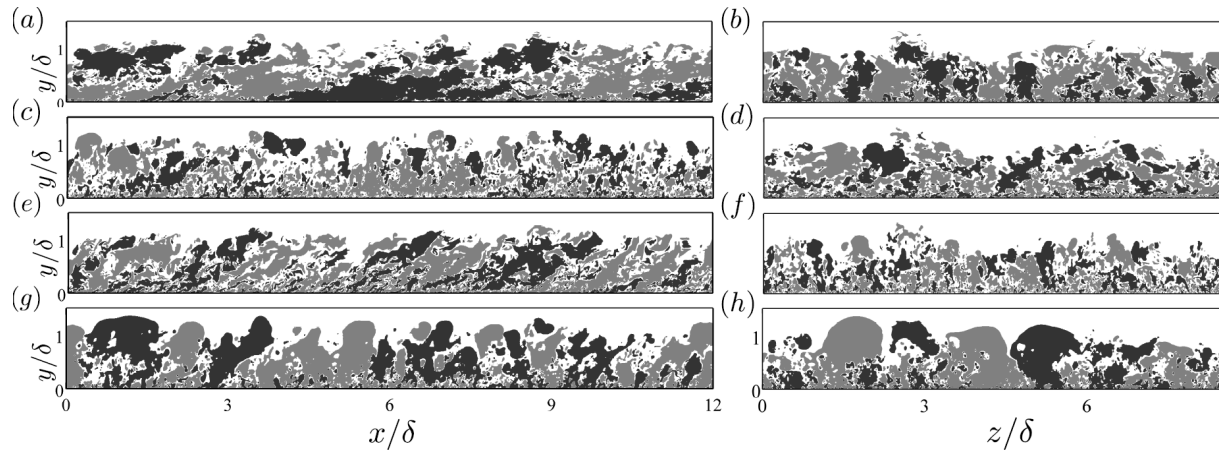


**Figure 4.** Instantaneous sections of the fluctuations:  $u^+$  (a, b),  $v^+$  (c, d),  $w^+$  (e, f),  $p^+$  (g, h). (a, c, e, g) are the  $x - y$  sections for  $Re_\theta = 5800 - 6600$ . (b, d, f, h) are the  $z - y$  sections at  $Re_\theta = 5800$ . Fluctuations are normalized with the friction velocity, and the coordinates are normalized with  $\delta_{99}$  at  $Re_\theta = 5800$ . Dark grey areas are below  $-0.5$  wall units, and lighter areas above  $+0.5$ .

#### 4. Conclusions

We have introduced the concept of the effective dimensionless length  $\tilde{x}$  in order to characterize the accommodation length needed for the large-scale structure of the flows to converge from artificial tripping methods to nominal values, resulting in lengths about  $\tilde{x} \approx 4$ . This is especially severe in the case of high  $Re_\theta$  in which the flow may not achieve the equilibrium by the end of the physical domain. In order to perform a direct numerical simulation of a boundary layer at high  $Re_\theta$ , an auxiliary simulation is conducted using relatively coarse resolution, and resolving correctly the large scales of the flow. The computational penalization of this auxiliary boundary layer is about 10% of the total time. It turns out that even at this low resolution the small scales are essentially well-resolved.

A preliminary analysis of the statistics of this new simulation has been conducted. Integral parameters, such as  $c_f$  and the shape factor, are within the scatter of the available experiments and numerical data sets. The same is true of the velocity fluctuations. At this relatively high Reynolds number, the mean profile exhibits a clear logarithmic region, and the fluctuations have been compared with the numerical channel at similar Reynolds numbers. Velocity fluctuations clearly show a weak dependence with the  $Re_\tau$  at the buffer layer, failing the classical scaling with the friction velocity  $u_\tau$ . The new simulation confirms that the transverse velocity fluctuations are stronger in boundary layers than in channels. Energy density spectra also shows the large-scale structure footprint near the wall. Boundary layer and channel kinetic energy spectra are compared in that near-wall region, revealing that the structures for channels are somewhat larger than boundary layers, but showing similar features for the small-scale structures.

## Acknowledgments

This research used resources of the Argonne Leadership Computing Facility at Argonne National Laboratory, which is supported by the Office of Science of the U.S. Department of Energy under contract DE-AC02-06CH11357. The work at the UPM was funded by CICYT under grant TRA2009-11498, and by the European Research Council under grant ERC-2010.AdG-20100224. J.A. Sillero was supported by an FPU fellowship from the UPM.

## References

- LUND, T. S., WU, X. & SQUIRES, K. D. 1998 Generation of Turbulent Inflow Data for Spatially-Developing Boundary Layer Simulations. *J. Comput. Phys.* **140**, 233–258
- HOYAS, S. & JIMÉNEZ, J. 2006 Scaling of the velocity fluctuations in turbulent channels up to  $Re_\tau = 2003$ . *Phys. Fluids* **18**, 011702
- JIMÉNEZ, J., HOYAS, S., SIMENS, M. P. & MIZUNO, Y. 2010 Turbulent boundary layers and channels at moderate Reynolds number. *J. Fluid Mech.* **657**, 335–360
- JIMÉNEZ, J. & HOYAS, S. 2008 Turbulent fluctuations above the buffer layer of wall-bounded flows. *J. Fluid Mech.* **611**, 215–236
- JIMÉNEZ, J., DEL ÁLAMO, J. C. & FLORES, O. 2004 The large-scale dynamics of near-wall turbulence. *J. Fluid Mech.* **505**, 179–199
- SIMENS, M. P., JIMÉNEZ, J., HOYAS, S. & MIZUNO, Y. 2009 A high-resolution code for turbulent boundary layers. *J. Comput. Phys.* **228**, 4218–4231
- DE GRAAFF, D. B. & EATON, J. K. 2000 Reynolds number scaling of the flat-plate turbulent boundary layer. *J. Fluid Mech.* **422**, 319–346
- OSTERLUND, J. M., JOHANSSON, A. V., NAGIB, H. M. & HITES, M. 2000 A note on the overlap region in turbulent boundary layers. *Phys. Fluids* **12**, 1–4
- SCHLATTER, P. & ÖRLÜ, R. 2010 Assessment of direct numerical simulation data of turbulent boundary layers. *J. Fluid Mech.* **659**, 116–126
- PURTELL, L. P., KLEBANOFF, P. S. & BUCKLEY, F. T. 1981 Turbulent boundary layers at low Reynolds numbers. *Phys. Fluids* **24**, 802–811
- ERM, L. P. & JOUBERT, P. N. 1991 Low-Reynolds-number turbulent boundary layers. *J. Fluid Mech.* **230**, 1–44
- HOYAS, S. & JIMÉNEZ, J. 2008 Reynolds number effects on the Reynolds-stress budgets in turbulent channels. , *Phys. Fluids* **20**, 101511
- TOWNSEND, A.A. 1976 *The structure of turbulent shear flow*. 2nd ed. (Cambridge U. Press, Cambridge)